Strong enhancement of the Breit-Wigner-Fano Raman line in carbon nanotube bundles caused by plasmon band formation

Chaoyang Jiang,[1] Kris Kempa,[2] Jialong Zhao,[1] Ulrich Schlecht,[3] Ute Kolb,[1] Thomas Basché,[1] Marko Burghard,[3] and Alf Mews[1,*]

[1]*Institut für Physikalische Chemie, Universität Mainz, D-55099 Mainz, Germany*
[2]*Department of Physics, Boston College, Chestnut Hill, Massachusetts 02467*
[3]*Max-Planck-Institut für Festkörperforschung, Heisenbergstrasse 1, D-70569 Stuttgart, Germany*
(Received 4 September 2002; published 25 October 2002)

We investigate the origin of the Breit-Wigner-Fano line in the Raman spectra of individual single-walled carbon nanotubes and their bundles. Using confocal Raman microscopy and atomic-force microscopy we found that the Breit-Wigner-Fano line intensity increases strongly with the bundle thickness. We confirmed this result by Raman investigations of partially decomposed bundles, which were additionally investigated by transmission electron microscopy. Our random-phase approximation based theory, which identifies the Breit-Wigner-Fano line as an excited band of plasmon-phonon modes, is fully consistent with the experimental results.

Carbon nanotubes are molecular wires that have attracted increasing attention in the fields of chemistry, physics, electronics, as well as material science.[1,2] Devices such as room temperature transistors and chemical sensors made from single-walled carbon nanotubes (SWCNTs) have shown the potential of this material for future nanoengineering.[3,4] Despite the progress towards reliable devices, a correlation between the structure of SWCNTs and their electronic properties is difficult to establish, because SWCNT samples produced by large-scale preparation techniques are very inhomogeneous. Depending on their chirality, the individual tubes can be metallic or semiconducting. Moreover, they usually appear in bundles containing different kinds of tubes with possible electronic interaction. Therefore, it is important to study the structure and electronic properties of individual SWCNT bundles in detail.

Raman spectroscopy has proven to be a powerful tool to probe vibrational modes and electronic properties of SWCNTs.[5] The three most dominant features in Raman spectra are the radial-breathing mode (RBM) in the low-frequency region ($100–200$ cm^{-1}), a vibration related to disordered carbon (D line) around 1300 cm^{-1}, and the G lines between $1580–1590$ cm^{-1} that originate from the tangential vibrations of the carbon atoms. For metallic SWCNTs an additional band close to the doublet of G lines (~ 1550 cm^{-1}) can be observed, which can be well fitted by a Breit-Wigner-Fano (BWF) line shape.[6,7] This band results from coupling of phonons to the electronic continuum of the metallic tubes[8] and is commonly used to distinguish between metallic and semiconducting SWCNTs. However, the nature of this coupling has not been fully clarified until now.

It has been shown that the BWF band is sensitive to the local environment because the intensity is different in chemically modified tubes[9] and tubes adsorbed on metal particles, i.e., in surface-enhanced resonance Raman scattering.[10] The results of chemical doping experiments of SWCNTs could only be explained by the assumption that individual tubes do not show a BWF line at all.[11] However, Raman experiments on individual SWCNTs revealed that the BWF line can also be seen in single nanotubes and that the relative intensity depends on the tube diameter.[12]

In this Rapid Communication we show that the intensity of the BWF line is strongly enhanced in bundles of SWCNTs due to the formation of a band of plasmons. We correlate the structural and electronic properties of SWCNTs by investigating the same individual bundles with confocal Raman microscopy and confocal Raman spectroscopy in combination with atomic-force microscopy (AFM) and transmission electron microscopy (TEM). Moreover, we show results of AFM manipulation used to decompose thicker bundles into smaller ones, resulting in a decrease of the BWF/G band intensity ratio. Finally, we present a theory to explain the experimental results.

In order to address the same individual bundles by AFM, TEM, and Raman microscopy, the SWCNTs (Carbolex®, Lexington USA) were deposited on surface-modified 20-nm-thick Si_3N_4 membranes with position markers.[13] AFM images were acquired with a Digital Instruments Nanoscope IIIA in tapping mode and the manipulation of the bundles was performed with standard silicon tips. TEM pictures were taken with a Phillips EM-420 equipped with a LaB_6 filament and operated at 120 kV. Raman microscopy was performed with a modified inverted Zeiss microscope as described in detail elsewhere.[14]

After spatial selection it is important to distinguish between metallic and semiconducting tubes. In resonance Raman experiments,[15] it is in principle possible to selectively address only one type of tubes by tuning the excitation wavelength to an electronic transition of either the metallic or semiconducting tubes. Here, we choose a wavelength of 647.1 nm to excite mainly the first electronic transition E_{11}^M of the metallic tubes.[16] However, from theory it is known that this energy (1.92 eV) is also in resonance with the third electronic transition E_{33}^S of semiconducting tubes between 1.6 and 1.8 nm in diameter.[17] Therefore, in addition to the excitation energy, the diameter needs to be known to clearly distinguish between resonantly excited metallic and semiconducting tubes.
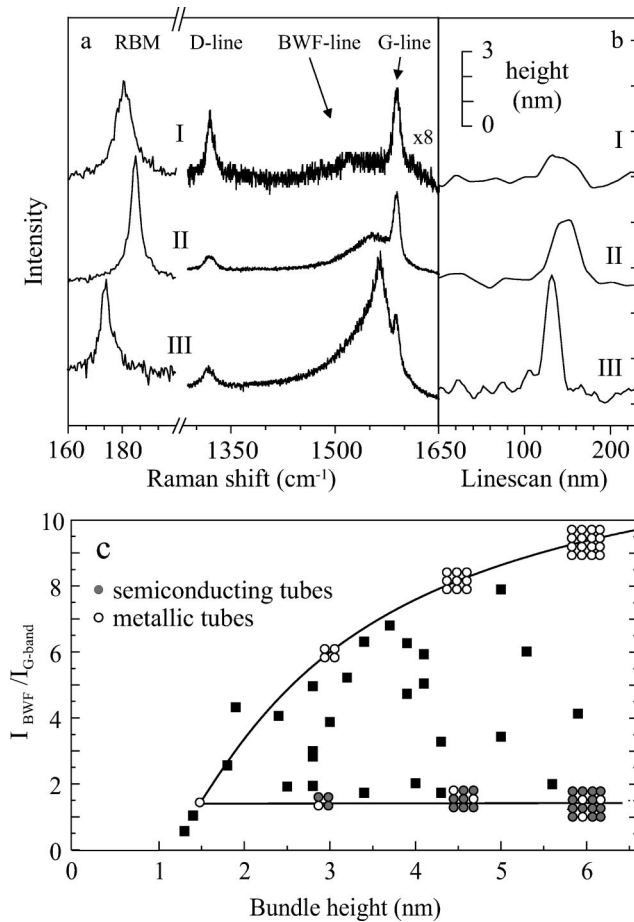
FIG. 1. Raman spectra (a) and AFM line scan profiles (b) of SWCNT bundles with different thickness. The RBM frequencies for I, II, and III are $\omega_I = 180$ cm^{-1}, $\omega_{II} = 184$ cm^{-1}, and $\omega_{III} = 174$ cm^{-1} with a respective FWHM of 6.7, 3.3, and 3.6 cm^{-1}. The respective AFM heights are 1.3 nm, 2.8 nm, and 5 nm, while the width of the AFM profile is mainly given by the tip geometry. (c) Relative intensity of the BWF line vs G line for 27 different bundles. The relative BWF intensity is always weak for thin bundles or individual tubes but varies for thicker bundles. The solid lines are guides to the eye, and show estimated relative intensities for pure metallic bundles and bundles containing isolated or noninteracting metallic tubes.

The diameter of the investigated SWCNTs can be obtained from Raman measurements by the RBM frequency using the relationship: $\omega_{RBM}(\text{cm}^{-1}) = 248/d(\text{nm})$.[17] From 56 thin bundles or individual tubes with only one single RBM we determined a diameter distribution centered at 1.47 nm with a full width at half maximum (FWHM) of 0.25 nm. From these spectra we considered only those for the following discussion which are consistent with the observation of metallic tubes ($d < 1.5$ nm). This selection of a narrow diameter range is also necessary to concentrate on the bundle effects because it practically eliminates the effect of different individual tube diameters on the relative BWF-line intensity.[12]

Figure 1(a) shows the Raman spectra of three different SWCNT (bundles) (I, II, and III). The AFM height of SWCNT No. I [Fig. 1(b)] is consistent with a single nano-
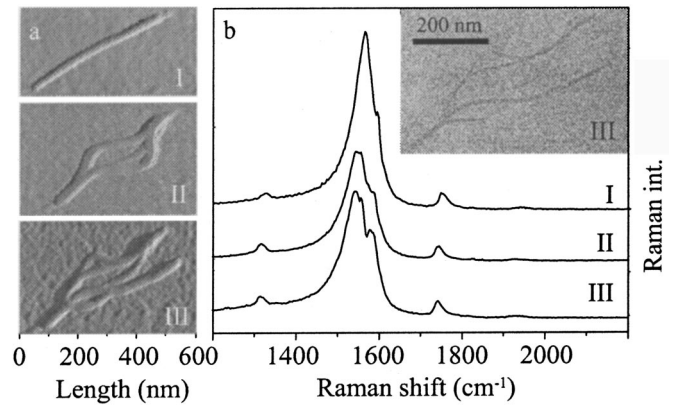

FIG. 2. (a) AFM and (b) Raman spectra at different stages of bundle decomposition. The relative intensity of BWF line decreases due to decreasing intrabundle interaction. Inset: TEM image of the SWCNT bundle after manipulation.

tube, although there is still a possibility of laterally adjacent tubes which cannot be resolved by AFM. However, the line scans of II and III clearly show that these are bundles even though the corresponding Raman spectra show a single RBM. Therefore, the investigated bundles either consist of similar tubes or, more likely, only a fraction of the tubes within the bundle can be resonantly excited with the excitation energy of 1.92 eV.

Most prominently, it can be seen that the intensity ratio of BWF vs G line (relative intensity) changes considerably with the bundle thickness, while the diameter of the resonantly excited tubes is quite similar, as judged from the RBM frequency. There is a strong enhancement of this ratio for some bundles, such as for (III) in Fig. 1(a), which could be due to increasing interaction of metallic tubes within the bundles. Therefore, we have measured the AFM height and the Raman spectra of 27 different bundles and fitted them with a BWF line at ~ 1560 cm^{-1} and a single Lorentzian to account for the G line at ~ 1590 cm^{-1}. The results shown in Fig. 1(c) clearly demonstrate that the relative intensity is always weak for thin bundles and is, in principle, increasing with bundle thickness. The reason why not all thick bundles show a strong relative intensity can be understood by the fact that on average only a third of the SWCNTs is metallic. Therefore, even thick bundles can contain isolated or at least noninteracting metallic tubes and hence show weak relative intensity.

To further investigate the effect of intertube interaction upon the Raman spectra, we manipulated SWCNT bundles with an AFM tip. Since it has already been demonstrated that an AFM tip can bend and buckle SWCNTs (Ref. 18) we used this technique to partly separate a big bundle into several small bundles and/or single nanotubes and compared the Raman spectra of the same SWCNTs before and after the decomposition.

Figure 2 shows Raman spectra as well as AFM and TEM images of the same individual bundle at two consecutive stages of decomposition. Before manipulation the bundle is straight with a length of 500 nm [Fig. 2(a), I] which is basically the spatial resolution in the Raman images. The corre-

sponding Raman spectrum [Fig. 2(b), I] shows a very strong BWF line and the G line can only be observed as a shoulder at 1590 cm^{-1}. By AFM manipulation, this bundle could obviously be divided over a length of about 200 nm [Fig. 2(a), II]. Since this is within the range of the spatial resolution of the optical microscope, the Raman spectrum [Fig. 2(b), II] originated from the same bundle which is now partially decomposed. While a pure bending of the SWCNTs did not lead to a noticeable change of the Raman spectra (not shown), the BWF/G-line ratio is decreased as a result of bundle decomposition in Fig. 2(a)/(b) (II). This effect becomes even more pronounced when the bundle is decomposed further [Fig. 2(a), III]. Now the G line at 1590 cm^{-1} can clearly be resolved [Fig. 2(b), III].

Since the lateral resolution of the AFM images is restricted by the AFM tip, additional information of the bundle geometry after decomposition can be gained from the TEM picture in the inset of Fig. 2(b). Although the contrast of this picture is low due to the Si_3N_4 substrate, it can be seen that the AFM manipulation leads to the formation of several smaller bundles and, therefore, to a system with reduced intertube interactions.

In order to understand the dependence of the BWF line intensity upon bundle thickness, the coupling of the phonons with the continuum of states needs to be known in detail. However, a general BWF fit yields unphysical (negative) values for the coupling parameters $1/q$,[6] which indicates that a better theory is needed. Therefore, we developed a theory for the spectral response of the electron gas in the presence of phonon excitations for individual metallic SWCNTs and also for bundles. We employed the random phase approximation, and modeled the metallic SWCNT as a conductive cylinder (along z direction) of diameter d. Details of our calculation will be presented elsewhere.[19] The problem essentially reduces to a calculation of the screened Coulomb interaction via the corresponding Dyson equation, which yields the following dielectric function

$$\varepsilon(\Omega,Q) = \frac{\omega^2 - \omega_{LO}^2}{\omega^2 - \omega_{TO}^2} + v(Q)\Pi_0(\Omega,Q). \qquad (1)$$

Here Ω and Q are, respectively, the frequency and the z component of the wave vector of a plasmon in Fermi units ($E_F = 8.18$ eV, $k_F = 1.47$ Å^{-1}). The first term in Eq. (1) is the well-known Lyddane-Sachs-Teller phonon contribution,[20] with ω_{LO} and ω_{TO} the upper and lower frequencies of the G lines, respectively. The second term is the electron-gas contribution with the bare Coulomb interaction within the bundle given by $v(Q) = \Sigma_{pl} v_{pl} \exp[i\mathbf{K} \cdot \mathbf{B}]$, with $(\mathbf{K},Q)$ the plasmon wave, and $\mathbf{B} = (pa_x, la_y)$ the bundle lattice vector (p,l are integers). $v_{pl} = (4/\pi^2 a^* n) K_m(Q,A) I_m(Q,d)$ is the Coulomb potential of a single tube,[21,22] a^* the effective Bohr radius, n the linear electron density, $A = d$ for $p = l = 0$ (single tube), and $A = |B|$ otherwise. K_m and I_m are the modified Bessel functions and $\Pi_0(\Omega,Q)$ is the noninteracting susceptibility.[19,23]

The dispersion in the absence of phonon coupling ($\omega_{LO} = \omega_{TO} = 0$) is
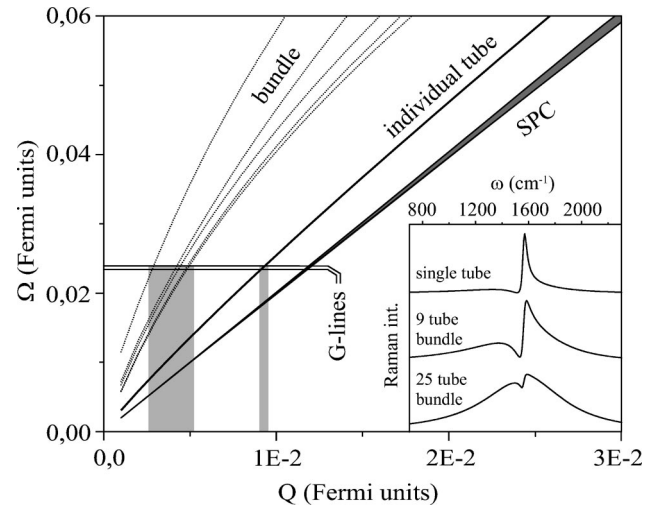

FIG. 3. Plasmon mode dispersions calculated from Eq. (2) for an individual metallic (9,0) tube and a bundle consisting of 25 tubes. Also shown are the edges of the single-particle continuum (SPC) and the frequencies of the G lines. Shaded areas show values of Q needed to assure the strong phonon-plasmon coupling. Inset shows the calculated Raman response (see text for details).

$$\Omega = 2Q \sqrt{\coth\frac{Q}{2v(Q)} + \frac{Q^2}{4} + 1}. \qquad (2)$$

Plasmon dispersions calculated from Eq. (2) are shown in Fig. 3. For a single metallic (9,0) nanotube there is only one plasmon mode while a wide band of plasmons is calculated for a bundle of 25 (9,0) SWCNTs. A few relevant modes from this band are shown as thin solid lines. This plasmon band forms as a result of the internanotube electrostatic interactions. A similar plasmon band was observed in a two-dimensional array of quantum wires.[24]

Hybrid plasmon-phonon modes form when these plasmon modes strongly interact with the phonon modes and this happens only in the vicinity of the crossing of the phonon energies (horizontal lines in Fig. 3) and plasmon lines. Coupling of the Raman photons to these plasmon-phonon modes can occur only if both the energies and momenta are conserved in the process. The momenta involved can be provided not only by the Raman photon itself (647 nm), which corresponds to Q of about 10^{-4}, but also by various inhomogeneities of the system, such as local defect density or finite nanotube (or bundle) length. For example, localized impurities separated by an averaged distance l, provide a discrete spectrum of momenta with Q roughly given by $n\pi/l$, with n integer. Since l is of the order of 300 nm (Ref. 25) the corresponding effective $Q \sim n \times 0.7 \times 10^{-3}$. We model the spectrum strength by a set of Gaussians located at these Q's, with amplitudes exponentially decreasing with n. Therefore only Q's corresponding to small n's provide an efficient coupling. From Fig. 3 it is clear that while this is insufficient to excite efficiently the plasmon-phonon mode of a single SWCNT, which requires $Q \sim 10^{-2}, n > 10$, the band of plasmon-phonons is available for the bundle of 25 nanotubes already for $n = 3$.

Coupling to plasmon-phonon modes should lead to a strong enhancement of the electromagnetic response. To show this, we calculate the corresponding Raman spectra[19] obtained essentially from the formula of Ref. 26. We replaced the relevant bare electron-phonon matrix element with the matrix element for the dressed combined electron-phonon interaction,[27] which involves the dielectric function [Eq. (1)], and accounts for the plasmon-phonon excitations. The result is shown in the inset of Fig. 3.

While for a single SWCNT (top) only one sharp resonance is present at the frequency of the longitudinal phonon mode ω_{LO}, a broad band evolves below ω_{LO} for SWCNT bundles of 9 (middle), and 25 nanotubes (bottom). The maximum of this broad band gains strength, and moves towards ω_{LO} with increasing number of tubes in the bundle. This is in good agreement with the experimental results shown in Fig. 1(a), where we could detect an upshift of the BWF maximum from 1540 cm^{-1} for spectrum No. I to 1567 cm^{-1} for spectrum No. III. It also explains the result shown in Fig. 2, since the decomposition of a bundle reduces the number of inter-acting SWCNTs in the resulting bundles. Finally, since formation of the broad BWF band is sensitive to the spectrum of available momenta, variations in nanotube length, local defect density, etc., this will lead to a large variation of the spectra from one SWCNT to another, which also can change the magnitude of the relative BWF line intensity.

In summary, we have combined confocal Raman microscopy, AFM, and TEM to correlate the structure and the electronic interaction of carbon nanotubes within bundles. We found that the intensity of the BWF line is strongly enhanced in thick bundles of carbon nanotubes and can be reduced upon mechanical bundle decomposition. Our theory explains all the experimental data, and shows that the BWF line in SWCNTs and their bundles is due to an excitation of plasmon modes coupled to phonons.

---

*Electronic address: alf.mews@uni-mainz.de

[1] S. Iijima, Nature (London) **354**, 56 (1991).

[2] R. Saito, G. Dresselhaus, and M. S. Dresselhaus, *Physical Properties of Carbon Nanotubes* (Imperial College Press, London, 1998).

[3] H.W.C. Postma, T. Teepen, Z. Yao, M. Grifoni, and C. Dekker, Science **293**, 76 (2001).

[4] J. Kong, N.R. Franklin, C. Zhou, M.G. Chapline, S. Peng, K. Cho, and H. Dai, Science **287**, 622 (2000).

[5] M.S. Dresselhaus and P.C. Eklund, Adv. Phys. **49**, 705 (2000).

[6] H. Kataura *et al.*, Synth. Met. **103**, 2555 (1999).

[7] L. Alvarez *et al.*, Chem. Phys. Lett. **316**, 186 (2000).

[8] S.D.M. Brown *et al.*, Phys. Rev. B **63**, 155414 (2001).

[9] Z. Yu and L. Brus, J. Phys. Chem. B **105**, 6831 (2001).

[10] P. Corio *et al.*, Phys. Rev. B **61**, 13 202 (2000).

[11] H. Kataura *et al.*, Mol. Cryst. Liq. Cryst. **340**, 757 (2000).

[12] A. Jorio *et al.*, Phys. Rev. B **65**, 155412 (2002).

[13] A. Mews *et al.*, Adv. Mater. **12**, 1210 (2000).

[14] F. Koberling, A. Mews, and Th. Basché, Adv. Mater. **13**, 672 (2001) .

[15] R. Saito, G. Dresselhaus, and M.S. Dresselhaus, Phys. Rev. B **61**, 2981 (2000).

[16] M.A. Pimenta *et al.*, Phys. Rev. B **58**, R16016 (1998).

[17] A. Jorio *et al.*, Phys. Rev. Lett. **86**, 1118 (2001).

[18] H.W.C. Postma, A. Sellmeijer, and C. Dekker, Adv. Mater. **12**, 1299 (2000).

[19] K. Kempa, Phys. Rev. B (to be published).

[20] Use of the Lyddane-Sachs-Teller relation is justified due to the curvature-induced polarization in SWCNT's: T. Dumitrica, C. M. Landis, B. I. Yakobson, Chem. Phys. Lett. **360**, 182 (2002).

[21] P. Longe and S.M. Bose, Phys. Rev. B **48**, 18 239 (1993).

[22] M.F. Lin, D.S. Chuu, and K.W.K. Shung, Phys. Rev. B **56**, 1430 (1997).

[23] Q. Li and S. Das Sarma, Phys. Rev. B **40**, 5860 (1989).

[24] S. Das Sarma and W. Lai, Phys. Rev. B **32**, 1401 (1985).

[25] Y. Fan, M. Burghard, and K. Kern, Adv. Mater. **14**, 130 (2002).

[26] A.G. Souza Filho *et al.*, Phys. Rev. B **63**, 241404 (2001).

[27] R. D. Mattluck, *A Guide to Feyman Diagrams in the Many-Body Problem* (Dover Publications, New York, 1992).